HHS Public Access

Author manuscript

Adv Healthc Mater. Author manuscript; available in PMC 2021 November 01.

Published in final edited form as:

Adv Healthc Mater. 2020 November ; 9(22): e2001226. doi:10.1002/adhm.202001226.

A 3D, Dynamically Loaded Hydrogel Model of the Osteochondral Unit to Study Osteocyte Mechanobiology

Rachel L. Wilmoth,
Department of Mechanical Engineering, University of Colorado Boulder, 1111 Engineering Drive, Boulder, CO 80309-0427

Virginia L. Ferguson,
Department of Mechanical Engineering, University of Colorado Boulder, 1111 Engineering Drive, Boulder, CO 80309-0427

BioFrontiers Institute, University of Colorado Boulder, 3415 Colorado Ave, Boulder, CO 80309-0596

Materials Science and Engineering, University of Colorado Boulder, 4001 Discovery Drive, Room N378, Boulder, CO 80309

Stephanie J. Bryant
Department of Chemical and Biological Engineering, University of Colorado Boulder, 3415 Colorado Ave, Boulder, CO 80309-0596

BioFrontiers Institute, University of Colorado Boulder, 3415 Colorado Ave, Boulder, CO 80309-0596

Materials Science and Engineering, University of Colorado Boulder, 4001 Discovery Drive, Room N378, Boulder, CO 80309

Abstract

Osteocytes are mechanosensitive cells that orchestrate signaling in bone and cartilage across the osteochondral unit. The mechanisms by which osteocytes regulate osteochondral homeostasis and degeneration in response to mechanical cues remain unclear. This study introduces a novel 3D hydrogel bilayer composite designed to support osteocyte differentiation and bone matrix deposition in a bone-like layer and to recapitulate key aspects of the osteochondral unit's complex loading environment. The bilayer hydrogel was fabricated with a soft cartilage-like layer overlaying a stiff bone-like layer. The bone-like layer contained a stiff 3D-printed hydrogel structure infilled with a soft, degradable, cellular hydrogel. The IDG-SW3 cells embedded within the soft hydrogel matured into osteocytes and produced a mineralized collagen matrix. Under dynamic compressive strains, near-physiological levels of strain were achieved in the bone layer (≤ 0.08%), while the cartilage layer borne the majority of the strains (>99%). Under loading, the model induced an osteocyte response, measured by prostaglandin E2, that was frequency, but not strain, dependent: a finding attributed to altered fluid flow within the composite. Overall, this new

Corresponding authors: stephanie.bryant@colorado.edu; virginia.ferguson@colorado.edu.

Conflict of Interest: The authors have no conflicts of interest.

hydrogel platform provides a novel approach to study osteocyte mechanobiology *in vitro* in an osteochondral tissue-mimetic environment.

Graphical Abstract

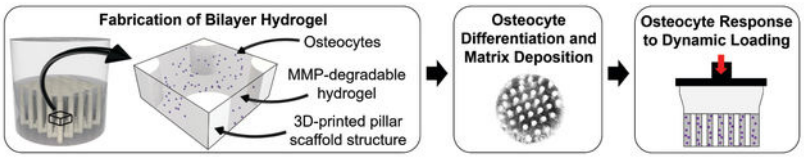

A novel 3D hydrogel bilayer composite is designed to support osteocyte differentiation, facilitate bone matrix deposition in a bone-like layer, and recapitulate key 3D aspects of the osteochondral unit's complex loading environment. This new hydrogel provides a novel platform to study osteocyte mechanobiology *in vitro* in an osteochondral tissue-mimetic environment.

Keywords

osteocyte; mechanobiology; osteochondral; hydrogel; mechanical loading

Osteocytes are mechanosensitive cells that help to orchestrate signaling in bone and cartilage across the osteochondral unit. Yet the mechanisms by which osteocytes regulate osteochondral homeostasis and degeneration in response to normal and aberrant mechanical cues remain unclear.[1,2] Currently, we lack sufficient means of studying osteocyte mechanobiology both *in vivo* and *in vitro.* This study aimed to develop an *in vitro* platform to study osteocyte mechanobiology within a subchondral bone mimetic. Our novel platform uses a 3D hydrogel bilayer composite designed to support osteocyte differentiation and bone matrix deposition in a bone-like layer and to recapitulate key aspects of the osteochondral unit's complex loading environment with a specific focus on achieving near-physiological levels of strain. Overall, this new osteochondral model may help to elucidate how changes in mechanical and hormonal cues affect homeostatic and degenerative processes in osteochondral tissues.

Osteocytes play a key role in regulating osteochondral homeostasis and degeneration. In bone, osteocytes detect hormonal and mechanical cues and respond by secreting signaling molecules that direct bone-forming osteoblasts and bone-resorbing osteoclasts.[3–6] In subchondral bone, osteocytes also engage in crosstalk with chondrocytes that reside in articular cartilage across the osteochondral interface.[1,2] During the progression of osteoarthritis, bone and cartilage undergo property changes; for example, cartilage permeability increases,[7] which in turn increases the fluid flow in bone and cartilage.[8,9] Osteocytes detect increased fluid flow in subchondral bone and then secrete signaling molecules that affect chondrocyte, osteoblast, and osteoclast activities that further contribute to osteochondral degeneration.[1,2,10–13] A 3D *in vitro* model that recapitulates the strain and fluid flow of the osteochondral unit would enable key questions to be answered about the osteocyte's role in regulating osteochondral homeostasis and degeneration.

Currently, 3D *in vitro* osteocyte models that capture relevant mechanical cues are insufficient. The loading environment in bone and, in particular the osteochondral unit, experiences matrix strains, typically between 0.001% and 0.3%,[3,14] and interstitial fluid flow. Studying osteocyte mechanobiology *in vivo*[15–21] is challenging due to the difficulty in isolating and controlling the effects of different mechanical stimuli on cells. While *in vitro* studies in 2D culture allow for tighter control over mechanical stimuli (*e.g.*, fluid flow) and have advanced our knowledge of osteocyte mechanotransduction,[22–25] to date, these studies lack 3D aspects of the *in vivo* environment.[26] To this end, researchers developed 3D osteocyte culture models to improve upon the limitations of 2D cultures.[27–33] For example, one study achieved mature osteocyte differentiation in a 3D collagen gel but this culture system lacked mechanical cues.[34] Other studies revealed new effects of direct matrix strains on osteocytes in 3D [27,29,35] such as strain-induced osteocyte regulation of osteoblast bone formation.[27] These prior studies applied matrix strains ranging from 0.4–10%, which exceed physiological levels of strain in bone. Other studies incorporated fluid perfusion into 3D cultures[15,28,30,32,36,37] and revealed, for example, the link between fluid-induced shear and gene expression of proteins that regulate osteoblast bone formation (e.g., sclerostin).[28] However, 3D models that adequately capture both physiologically-relevant matrix strains and fluid perfusion are limited.

Here, we designed a bilayer composite hydrogel to mimic the osteochondral unit and control strain within the cellular niche where the osteocytes reside. While numerous studies have developed bilayer scaffolds for osteochondral defect repair models (e.g.[38–46]), few studies examine osteocytes in these scaffolds. A representative image of a histological section of human osteochondral tissue (Figure 1A) illustrates articular cartilage overlaying a thin interfacial calcified cartilage layer, underlying cortical subchondral bone plate, and subchondral trabecular bone.[10,47,48] The osteochondral unit possesses a large mismatch in the compressive moduli between articular cartilage, ranging from 1–10 MPa,[49,50] and the subchondral bone, ranging from 1–10 GPa.[51,52] These disparate properties influence strain transfer from cartilage to bone during normal joint movement. To capture this difference, we fabricated a bilayer hydrogel with a soft cartilage-like layer overlaying a stiff bone-like layer. Because cells encapsulated in a 3D hydrogel, including bone cells, require soft and degradable hydrogels to form 3D interconnected cellular networks,[53] we introduced a stiff 3D-printed hydrogel structure into the bone layer to increase its composite modulus while maintaining a soft cellular niche. We designed the geometry of the 3D-printed structure to consist of vertical pillars which serve as stiff reinforcements to bear load, control strain and protect the cells within the cellular niche.[54] Rather than mimicking the modulus of bone, which is difficult to achieve in a 3D printed polymeric scaffold, we aimed to recapitulate the level of strain in bone with this osteochondral model. Discussed below are four aspects of this osteochondral model for the study of osteocyte mechanobiology: (1) fabrication of a bilayer hydrogel, (2) calculation of strain in each layer, (3) demonstration of osteocyte differentiation and bone matrix deposition, and (4) demonstration that loading induces an osteocyte response.

The bilayer composite was fabricated from poly(ethylene glycol) (PEG)-based hydrogels whose formulations were chosen to achieve functional differences in moduli that approach those of osteochondral tissues (Figure 1B). The 3D-printed structure was fabricated using

stereolithography and a PEG diacrylate resin whose material compressive modulus was 31.1 (1.2) MPa (i.e., mean (SD)). This 3D-printed PEG structure was chosen for its stiff mechanical properties, hydrophilicity, and cytocompatibility.[54,55] The 3D-printed structure was infilled with IDG-SW3 osteocytes encapsulated in a soft and degradable PEG hydrogel that supports osteocyte differentiation.[56] PEG was chosen as the base synthetic chemistry for it tunability, cytocompatibility, and ease of modifying with groups (e.g. norbornenes) that participate in thiol-ene click reactions and allow for facile incorporation of peptides (e.g. RGD) and peptide crosslinks. The hydrogel was made with crosslinks of matrix-metalloproteinase (MMP) sensitive peptides to enable cell-mediated degradation and tethered with RGD peptides to facilitate cell-hydrogel interactions. Over 35 days of static culture, the soft hydrogel supported cell viability (Figure 1C with live cells stained green by Calcein-AM and Figure S1 with dead cells stained red with ethidium homodimer) and cellular spreading (Figure 1C) with dendrite-like protrusions. The latter is important for creating an interconnected cellular system, known in bone as the lacunocanalicular network.[4] Some cell aggregation was observed, which is likely to have occurred prior to the encapsulation process,[57] but did not adversely affect cell viability. The compressive modulus of the acellular MMP-sensitive hydrogel was 8.8 (0.4) kPa, and after 35 days of differentiation the cell-laden hydrogel was 2.2 (0.2) kPa. The softer cell-laden hydrogel is attributed to several effects. At the time of encapsulation, cells can sequester crosslinker molecules prior to polymerization which lowers the effective crosslink density and hence stiffness.[58] After encapsulation, secretion of MMPs can lead to rapid degradation of the hydrogel before the cells have time to differentiate and deposit their own ECM.[57,59] The modulus of the 3D-printed structure infilled with the soft hydrogel (i.e. the bone layer shown in Figure 1B) was 2.4 (0.5) MPa. The cartilage layer was made from a PEG hydrogel containing non-degradable PEG-dithiol crosslinkers and a modulus of 2.9 (0.4) kPa.

We applied Hooke's Law to determine the relative transfer of strain to each layer when the bilayer composite is subjected to an applied compressive strain (Figure 1D). The strain in the cartilage layer was approximately twice the applied strain (Figure 1E): 20% applied strain resulted in 40 (0.012) % strain in the cartilage layer (Table S1). In contrast, strain in the bone layer was minimal compared to the applied strain (Figure 1F): 20% applied strain resulted in 0.066 (0.012) % strain in the bone layer (Table S1). We applied strains of 5, 10, or 20% and in each case, the cartilage layer took on > 99% of the applied strain while strain in the bone layer was consistently ≤ 0.08%. These results confirm near-physiological strains were achieved within the bone layer.

We evaluated two requirements of the cellular niche within this bilayer composite: mature osteocyte differentiation and bone matrix deposition. The IDG-SW3 cell line was derived from murine long bone chips and was chosen for the ability to differentiate from osteoblasts to late osteocytes and deposit a mineralized collagen matrix.[60] Over a 35-day static culture (Figure 2A), IDG-SW3 cells differentiated from osteoblasts to osteocytes. Connexin 43 was observed by punctate staining in the hydrogel (Figure 2B), which is consistent with connexin 43 staining in a 2D culture control (Figure 2C) and typical for connexin 43 (negative control images included in Figure S2).[61,62] Connexin 43 comprises hemichannels and gap junctions along the cell membrane and is essential for osteocyte function, survival, and differentiation.[63–65] Concomitant, normalized expression (NE) of osteocyte-related genes

Dmp1 and *Sost*, as measured by qPCR, increased over culture time (Figure 2D). DMP1 plays a role in hydroxyapatite formation and lacunocanalicular formation[5] and marks the beginning of the osteoblast to osteocyte transition.[60,66–68] Sclerostin (encoded by *Sost*), expressed by mature osteocytes, regulates osteoblast-mediated bone formation.[5,69]The NE of *Dmp1* and *Sost* at day 35 was significantly higher than both day 0 pre-encapsulated cells (*Dmp1*: $p = 0.002$, *Sost*: $p = 0.009$) and day 1 encapsulated cells (*Dmp1*: $p = 0.002$, *Sost*: $p = 0.022$). Collectively, these results indicate that the statically-cultured IDG-SW3 cells in the bone layer differentiated toward a mature osteocyte phenotype.

The deposition of bone matrix by the encapsulated osteocytes was also assessed after 35 days of differentiation in static culture. Matrix deposition was limited to the bottom layer, as evidenced by opaque coloration in images of the bilayer composite on day 35 (Figure 2E). Organic and inorganic components comprise bone matrix: the organic component includes mostly collagen type I while the inorganic component includes predominantly hydroxyapatite crystals, which are initially deposited as amorphous calcium phosphate.[47] The collagen serves as the organizational backbone for mineralization, following nucleation,[70] and binding[71–73] of hydroxyapatite crystals. We therefore assessed bone matrix deposition by 3D X-Ray microscopy (XRM) imaging and staining for calcium and collagen type I deposits in the bottom layer. XRM confirmed no detectable mineral content in the cartilage layer at any time point or in the bone layer on day 1. However, mineral was present through the bone layer by day 14 and further increased on day 35 (Figure 2F–G). The 3D printed pillars were visible by an absence of mineralization. Minimal difference was observed in the spatial distribution of deposited mineral, which suggests that the cellular-mediated mineral deposition was unimpacted by the 3D-printed structure. Calcium deposition was further confirmed by von Kossa staining of sections from glycol methacrylate (GMA)-embedded samples (Figure 2H–I). Collagen type 1 deposition was confirmed by immunohistochemical staining of sections from GMA-embedded samples (Figure 2J–K). GMA embedding limited extracellular staining; yet the positive staining for calcium and collagen type I within intracellular regions confirmed that the osteocytes produced bone matrix. Taken together, the bone layer of the composite hydrogel promoted both osteocyte differentiation and deposition of mineralized and collagenous matrix.

We next assessed the effect of loading on the osteocyte response by compressing the bilayer composite at varying applied strains (0, 5, 10, 20%) and frequencies (0.5, 1, 2 Hz) (Figure 3A). To determine whether osteocytes could sense and respond to an applied load in the 3D model, prostaglandin E_2 (PGE_2) was chosen as a measure of osteocyte response. PGE_2 is rapidly secreted by osteocytes, on the order of minutes,[74,75] in response to a mechanical stimulus (e.g., fluid flow[74,76] and compression[77]). Herein, PGE_2 was measured in the culture medium immediately after on hour of loading. Bilayer composite hydrogels were cultured between 35–43 days to first establish a bone matrix and mature osteocytes within the cellular niche. Then, on the final day of culture, hydrogels were dynamically loaded in a bioreactor for one hour. PGE_2 levels released into the culture medium immediately after loading were affected ($p < 0.0001$) by loading group (Figure 3B). We did not investigate loading of the infill hydrogel alone (i.e., without the stiff structure) due to its low modulus, which when placed in the bioreactor will lead to high tare strains imparted by the weight of the loading platens. All loading groups showed higher ($p < 0.05$) PGE_2 levels when

compared to the unloaded group. Pair-wise comparisons between loading groups revealed several interesting findings. There was no significant effect of strain for comparisons within the same frequency. Here, bone layer strains were 0.033% and 0.066% (Table S1) for applied strains of 10 and 20%, respectively. This suggests that a difference in strain of 0.033% experienced by the osteocytes was insufficient to further influence PGE_2 levels. However, there were differences with loading frequencies. PGE_2 levels increased from 1 to 2 Hz frequency at both 10% ($p < 0.0001$) and 20% ($p = 0.0003$) applied strain. But an opposite effect was observed where PGE_2 levels decreased with increased frequency from 0.5 Hz to 1 Hz at 20% applied strain ($p = 0.0013$). These findings suggest that in this culture system and with IDG-SW3 cells, the osteocyte PGE_2 response is more sensitive to loading frequency than strain magnitude.

We next added an inhibitor of COX2, NS-398, which is required for PGE_2 synthesis,[78] to evaluate load-induced osteocyte synthesis of PGE_2 (Figure 3C). NS-398 was added to the media in the unloaded control and for the condition with the highest PGE_2 concentration (10% strain, 2 Hz). In the absence of loading, osteocytes secreted low levels of PGE_2, which was further reduced ($p = 0.001$) by NS-398. NS-398 treatment abrogated ($p = 0.0002$) the load-induced PGE_2 levels, bringing the levels lower than the control samples without NS-398 ($p < 0.05$). These findings confirm that dynamic compressive loading, when applied to this composite hydrogel, induced PGE_2 synthesis by osteocytes.

While dynamic loading frequency elicited an osteocyte response via PGE_2 production, the magnitude of applied strain had no effect. The applied strains that are translated to the bone layer are small, which is consistent with *in vitro* 2D studies that show bone cells are unaffected by cellular strains less than 0.5%.[79] Yet, tissue-level strains within bone range from 0.001–0.3% and rarely exceed 0.2%.[14] When bone is strained, fluid moves through the lacunocanalicular system and the elements that tether osteocytes to the canalicular walls are subjected to tension. This process amplifies the tissue-level strains on the cell's cytoskeleton by 10–100 fold.[11] Strain-amplification also occurs due to the softer pericellular matrix that surrounds osteocytes *in vivo*, where strain increases by 1.4–2.7×.[80] Thus, we postulate that osteocytes sense strain-induced mechanical cues when the environment leads to cellular strain amplification. In this study, we surmise that the effects dominated by frequency may be in part due to fluid flow-induced cellular strain amplification that occurs as fluid moves through the soft hydrogel and adjacent to the embedded osteocytes. Although the exact mechanisms remain to be determined, findings from this study indicate that osteocytes are more sensitive to fluid flow than physiologically relevant tissue-level strains, which is in agreement with computational models[11,81,82] and *in vitro* experiments[11,83].

Our findings also suggest that the bilayer composite hydrogel can generate fluid-induced flow in the bone layer despite the low strains that are transferred to the hydrogel. Increases in frequency during unconfined compression of cartilage amplify the velocity of interstitial fluid.[84] In our system, unconfined compression of the bilayer composite generated large strains (~10–40%) in the cartilage layer. As the cartilage layer hydrogel contains 98% water and PEG hydrogels exhibit poroelastic behavior,[85–87] fluid movement in the cartilage layer will be, in part, forced downward and into the bone layer when compressed.[38] This

phenomenon is similar to fluid movement across the osteochondral interface between articular cartilage and subchondral bone when the unit is compressed.[8] We expect the magnitude of fluid flow to be relatively low within the hydrogel (e.g., 1–10 nm second^{-1}[38]) based on previous computational modeling of bilayer hydrogels where the bone layer underwent ~1% strain. Contrarily, lacunocanalicular flow in bone is predicted to have velocities of ~300 nm second^{-1}.[88] This, in combination with the finding that strains did not affect load-induced PGE_2 synthesis by osteocytes, further points to the hypothesis that our 3D model may enable cellular strain amplification when subjected to frequency-induced small changes in fluid flow. While fluid flow magnitudes are difficult to determine, future studies will utilize experiments and computational modeling to evaluate this complex loading environment.

In conclusion, this study presents a new 3D model of the osteochondral unit to study the effects of simulated *in vivo* loading on osteocytes. Near-physiological levels of strain were achieved in the bone layer of the composite hydrogel. Further, the model induced an osteocyte response that was frequency, but not strain, dependent; we attribute the cellular response to altered fluid flow and possibly cellular strain amplification, which is observed *in vivo*. Our model will empower *in vitro* studies of osteocytes in a highly controlled system that mimics the mechanical environment of the osteochondral unit's subchondral bone plate. While this study used an MMP-sensitive PEG hydrogel, other hydrogels that support osteocyte differentiation could readily be infilled into the stiff 3D-printed structure and attain near-physiological levels of strain in the bone-like layer. Other environmental considerations that are known to influence osteocytes could be studied within this model, which include pH,[89] oxygen tension,[90] drug treatment,[91] hormone levels,[92,93] or inflammatory mediators.[94] Further, this unique model may generate new insights into the osteocyte's role in propagating osteoarthritis progression in response to the changes in fluid flow.[7,8] Even further, chondrocytes can be encapsulated the top layer and osteocyte-chondrocyte crosstalk —a key part of osteochondral homeostasis and degeneration—can be investigated under different loading or inflammatory environments.

Experimental Section

Details of all methods are provided in the Supporting Information and all materials used are provided in Table S2. A custom-built stereolithography system[54] was used to 3D-print the stiff structure (Figure S3). A rectangular structure (3 mm x 3 mm x 1.5 mm) was designed with an array of 250 μm diameter pillars occupying 25% of the volume and resulting in a 75% void volume. A lattice on top and bottom connects the pillars and allows fluid flow between the layers. The resin was comprised of poly(ethylene glycol) diacrylate (700 g/mol) and pentaerythritol tetrakis(3-ercaptopropionate) mixed at a ratio of 99:1 by weight with 2-(2-hydroxyphenyl)-benzotriazole derivative (10 mg ml^{-1}, Tinuvin CarboProtect), Diphenyl-(2,4,6-trimethylbenzoyl)phosphine oxide (0.05 wt%, TPO) as a photoinitiator, and 2,20-Azobis(2-methylpropionitrile) (0.56 mg ml^{-1}, AIBN) for thermal post-curing. The structure was printed in 10 μm thick layers and each layer was exposed to 405 nm light for 12 seconds at an average intensity of 76 mW cm^{-2}. Post-printing, structures were briefly washed in 100% ethanol to remove the resin and then placed in an oven at a temperature of 105°C under vacuum for 1 hour. The structures were soaked in 100% ethanol for 72 hours to

remove any unreacted monomers within the material and then sterilized in 70% ethanol for 48 hours.

The bilayer hydrogel was fabricated by first infilling the 3D-printed structure with the MMP-sensitive cellular hydrogel containing IDG-SW3 cells (at a concentration of 80×10^6 cells ml^{-1} of hydrogel precursor) and then forming an overlying acellular layer using established protocols.[95] The compressive modulus values were obtained by testing cylindrical samples in unconfined compression.[56] Throughout static culture, samples were stained using a Live/Dead assay (Calcein-AM and ethidium homodimer) and imaged using confocal microscopy.[56] After 35 days of culture, samples were collected for: immunohistochemical and histological staining for connexin 43, collagen type I, and calcium[96]; RNA extraction and qPCR analysis; X-Ray Microscope imaging of mineralization; and dynamic loading using a custom bioreactor.[97–100] After loading, PGE_2 in the media was measured using a standard ELISA. Data were analyzed for statistical significance using either a two-tailed t-test (mineral fraction) or a one- or two-way analysis of variance followed by Tukey's post hoc analysis (α=0.05). Data are presented as mean (standard deviation) in the text, while graphical results are presented as box plots or as a mean with standard deviations as error bars.

Supplementary Material

Refer to Web version on PubMed Central for supplementary material.

Acknowledgments

The authors acknowledge technical support from Sadhana Sharma (hydrogel fabrication and culture), A. Camila Uzcategui (3D printing); Kristine Fischenich (XRM methods development and scanning, statistics advice), Sarah Schoonraad (immunohistochemistry methods development), Victor Crespo (single 3D-printed pillar modulus values); and Jennifer Coulombe (statistics advice). We thank Professor Corey Neu for the use of A1R Nikon Confocal System and Professor Vanessa Sherk for the use of the Leica HistoCore Autocut microtome. The research reported in this publication was supported by the National Institute of Arthritis and Musculoskeletal and Skin Diseases of the National Institutes of Health under the Award 1R21AR069791-01A1 and 1R01AR069060-01A1. RLW was supported on an NIH/NIA National Institute of Aging Integrative Physiology of Aging Training Grant under Award T32AG000279-16A1. The content in this publication is solely the responsibility of the authors and does not necessarily represent the official views of the NIH.

References

[1]. Findlay DM, Kuliwaba JS, Bone Research 2016, 4, 16028. [PubMed: 27672480]

[2]. Funck-Brentano T, Cohen-Solal M, Cytokine & Growth Factor Reviews 2011, 22, 91. [PubMed: 21596615]

[3]. Schaffler MB, Cheung W-Y, Majeska R, Kennedy O, Calcified Tissue International 2014, 94, 5. [PubMed: 24042263]

[4]. Bonewald LF, Journal of Bone and Mineral Research 2011, 26, 229. [PubMed: 21254230]

[5]. Klein-Nulend J, Bakker AD, Bacabac RG, Vatsa A, Weinbaum S, Bone 2013, 54, 182. [PubMed: 23085083]

[6]. Alliston T, Current Osteoporosis Reports 2014, 12, 366. [PubMed: 24894149]

[7]. Hwang J, Bae WC, Shieu W, Lewis CW, Bugbee WD, Sah RL, Arthritis & Rheumatism 2008, 58, 3831. [PubMed: 19035476]

[8]. Stender ME, Regueiro RA, Ferguson VL, Computer Methods in Biomechanics and Biomedical Engineering 2016, 1.

[9]. Stender ME, Carpenter RD, Regueiro RA, Ferguson VL, Journal of Biomechanics 2016, DOI 10.1016/j.jbiomech.2016.09.024.

[10]. Burr DB, Current Opinion in Rheumatology 1998, 10, 256. [PubMed: 9608330]

[11]. Fritton SP, Weinbaum S, Annual Review of Fluid Mechanics 2009, 41, 347.

[12]. Hemmatian H, Bakker AD, Klein-Nulend J, van Lenthe GH, Curr Osteoporos Rep 2017, 15, 401. [PubMed: 28891009]

[13]. Mazur CM, Woo JJ, Yee CS, Fields AJ, Acevedo C, Bailey KN, Kaya S, Fowler TW, Lotz JC, Dang A, et al., Bone Res 2019, 7, 34. [PubMed: 31700695]

[14]. Fritton SP, McLeod KJ, Rubin CT, Journal of biomechanics 2000, 33, 317. [PubMed: 10673115]

[15]. Tanaka T, Hoshijima M, Sunaga J, Nishida T, Hashimoto M, Odagaki N, Osumi R, Aadachi T, Kamioka H, Journal of Bone and Mineral Metabolism; Tokyo 2018, 36, 519.

[16]. Lynch ME, Brooks D, Mohanan S, Lee MJ, Polamraju P, Dent K, Bonassar LJ, van der Meulen MCH, Fischbach C, Journal of Bone and Mineral Research 2013, 28, 2357. [PubMed: 23649605]

[17]. Lara-Castillo N, Kim-Weroha NA, Kamel MA, Javaheri B, Ellies DL, Krumlauf RE, Thiagarajan G, Johnson ML, Bone 2015, 76, 58. [PubMed: 25836764]

[18]. Lewis KJ, Frikha-Benayed D, Louie J, Stephen S, Spray DC, Thi MM, Seref-Ferlengez Z, Majeska RJ, Weinbaum S, Schaffler MB, Proceedings of the National Academy of Sciences 2017, 114, 11775.

[19]. Robling AG, Niziolek PJ, Baldridge LA, Condon KW, Allen MR, Alam I, Mantila SM, Gluhak-Heinrich J, Bellido TM, Harris SE, et al., Journal of Biological Chemistry 2008, 283, 5866. [PubMed: 18089564]

[20]. Holguin N, Brodt MD, Silva MJ, Journal of Bone and Mineral Research 2016, 31, 2215. [PubMed: 27357062]

[21]. Metzger CE, Brezicha JE, Elizondo JP, Narayanan SA, Hogan HA, Bloomfield SA, Bone 2017, 105, 26. [PubMed: 28782619]

[22]. Rath AL, Bonewald LF, Ling J, Jiang JX, Van Dyke ME, Nicolella DP, Journal of Biomechanics 2010, 43, 1560. [PubMed: 20189178]

[23]. Liu C, Zhao Y, Cheung W-Y, Gandhi R, Wang L, You L, Bone 2010, 46, 1449. [PubMed: 20149907]

[24]. Galea GL, Sunters A, Meakin LB, Zaman G, Sugiyama T, Lanyon LE, Price JS, FEBS Letters 2011, 585, 2450. [PubMed: 21723865]

[25]. Atkins GJ, Rowe PS, Lim HP, Welldon KJ, Ormsby R, Wijenayaka AR, Zelenchuk L, Evdokiou A, Findlay DM, Journal of Bone and Mineral Research 2011, 26, 1425. [PubMed: 21312267]

[26]. Zhang C, Bakker AD, Klein-Nulend J, Bravenboer N, Current Osteoporosis Reports 2019, 17, 207. [PubMed: 31240566]

[27]. Vazquez M, Evans BAJ, Riccardi D, Evans SL, Ralphs JR, Dillingham CM, Mason DJ, Front Endocrinol (Lausanne) 2014, 5, DOI 10.3389/fendo.2014.00208.

[28]. Sun Q, Choudhary S, Mannion C, Kissin Y, Zilberberg J, Lee WY, Bone 2018, 106, 148. [PubMed: 29066313]

[29]. Takemura Y, Moriyama Y, Ayukawa Y, Kurata K, Rakhmatia YD, Koyano K, Journal of Biomedical Materials Research Part A 2019, 107, 815. [PubMed: 30578719]

[30]. Choudhary S, Sun Q, Mannion C, Kissin Y, Zilberberg J, Lee WY, Tissue Engineering Part A 2018, 24, 458. [PubMed: 28594289]

[31]. Kurata K, Heino TJ, Higaki H, Väänänen HK, Journal of Bone and Mineral Research 2006, 21, 616. [PubMed: 16598382]

[32]. Spatz JM, Wein MN, Gooi JH, Qu Y, Garr JL, Liu S, Barry KJ, Uda Y, Lai F, Dedic C, et al., Journal of Biological Chemistry 2015, 290, 16744. [PubMed: 25953900]

[33]. Mc Garrigle M, Haugh M, Voisin M, McNamara L, European Cells and Materials 2016, 31, 323. [PubMed: 27215740]

[34]. Bernhardt A, Weiser E, Wolf S, Vater C, Gelinsky M, Tissue Engineering Part A 2019, 25, 1347. [PubMed: 30648477]

[35]. Lynch ME, Chiou AE, Lee MJ, Marcott SC, Polamraju PV, Lee Y, Fischbach C, Tissue Engineering Part A 2016, 22, 1006. [PubMed: 27401765]

[36]. Wang W, Sarazin BA, Kornilowicz G, Lynch ME, Frontiers in Endocrinology 2018, 9, DOI 10.3389/fendo.2018.00352.

[37]. You L, Temiyasathit S, Tao E, Prinz F, Jacobs CR, Cellular and Molecular Bioengineering 2008, 1, 103.

[38]. Aziz AH, Eckstein K, Ferguson VL, Bryant SJ, Journal of Tissue Engineering and Regenerative Medicine 2019, 13, 946. [PubMed: 30793536]

[39]. Galperin A, Oldinski RA, Florczyk SJ, Bryers JD, Zhang M, Ratner BD, Advanced Healthcare Materials 2013, 2, 872. [PubMed: 23225568]

[40]. Gan D, Wang Z, Xie C, Wang X, Xing W, Ge X, Yuan H, Wang K, Tan H, Lu X, Advanced Healthcare Materials 2019, 8, 1901103.

[41]. Kim BJ, Arai Y, Choi B, Park S, Ahn J, Han I-B, Lee S-H, Journal of Industrial and Engineering Chemistry 2018, 61, 295.

[42]. Lin D, Cai B, Wang L, Cai L, Wang Z, Xie J, Lv Q, Yuan Y, Liu C, Shen SGF, Biomaterials 2020, 253, 120095. [PubMed: 32445809]

[43]. Liu K, Liu Y, Duan Z, Ma X, Fan D, Sci. China Technol. Sci. 2020, DOI 10.1007/s11431-020-1597-4.

[44]. Liu X, Wei Y, Xuan C, Liu L, Lai C, Chai M, Zhang Z, Wang L, Shi X, Advanced Healthcare Materials n.d, n/a, 2000076.

[45]. Steinmetz NJ, Aisenbrey EA, Westbrook KK, Qi HJ, Bryant SJ, Acta Biomaterialia 2015, 21, 142. [PubMed: 25900444]

[46]. Zhu X, Chen T, Feng B, Weng J, Duan K, Wang J, Lu X, ACS Biomater. Sci. Eng. 2018, 4, 3534.

[47]. Burr DB, Akkus O, in Basic and Applied Bone Biology, Elsevier, 2014, pp. 3–25.

[48]. Lories RJ, Luyten FP, Nature Reviews Rheumatology 2011, 7, 43. [PubMed: 21135881]

[49]. Chan DD, Cai L, Butz KD, Trippel SB, Nauman EA, Neu CP, Scientific Reports 2016, 6, 19220. [PubMed: 26752228]

[50]. Wahlquist JA, DelRio FW, Randolph MA, Aziz AH, Heveran CM, Bryant SJ, Neu CP, Ferguson VL, Acta Biomaterialia 2017, 64, 41. [PubMed: 29037894]

[51]. Choi K, Kuhn JL, Ciarelli MJ, Goldstein SA, Journal of biomechanics 1990, 23, 1103. [PubMed: 2277045]

[52]. Hargrave-Thomas E, van Sloun F, Dickinson M, Broom N, Thambyah A, Osteoarthritis and Cartilage 2015, 23, 1755. [PubMed: 26028136]

[53]. Aziz AH, Bryant SJ, Biotechnology and Bioengineering 2019, 116, 1523. [PubMed: 30776309]

[54]. Uzcategui AC, Muralidharan A, Ferguson VL, Bryant SJ, McLeod RR, Adv. Eng. Mater. 2018, 20, 1800876. [PubMed: 30766445]

[55]. Aisenbrey EA, Tomaschke A, Kleinjan E, Muralidharan A, Pascual-Garrido C, McLeod RR, Ferguson VL, Bryant SJ, Macromolecular Bioscience 2018, 18, 1700267.

[56]. Aziz AH, Wilmoth RL, Ferguson VL, Bryant SJ, ACS Appl. Bio Mater. 2020, 3, 1666.

[57]. Schneider MC, Chu S, Sridhar SL, de Roucy G, Vernerey FJ, Bryant SJ, ACS Biomater. Sci. Eng. 2017, 3, 2480. [PubMed: 29732400]

[58]. Chu S, Maples MM, Bryant SJ, Acta Biomaterialia 2020, 109, 37. [PubMed: 32268243]

[59]. Aisenbrey EA, Bryant SJ, Journal of Biomedical Materials Research Part A 2018, 106, 2344. [PubMed: 29577606]

[60]. Woo SM, Rosser J, Dusevich V, Kalajzic I, Bonewald LF, J Bone Miner Res 2011, 26, 2634. [PubMed: 21735478]

[61]. Langhorst H, Jüttner R, Groneberg D, Mohtashamdolatshahi A, Pelz L, Purfürst B, Schmidt-Ott KM, Friebe A, Rathjen FG, Disease Models & Mechanisms 2018, 11, dmm032128. [PubMed: 29361518]

[62]. Balla P, Maros ME, Barna G, Antal I, Papp G, Sapi Z, Athanasou NA, Benassi MS, Picci P, Krenacs T, PLOS ONE 2015, 10, e0125316. [PubMed: 25933380]

[63]. Plotkin LI, Actual osteol 2011, 7, 79. [PubMed: 22679450]

[64]. Gramsch B, Gabriel H-D, Wiemann M, Grümmer R, Winterhager E, Bingmann D, Schirrmacher K, Experimental Cell Research 2001, 264, 397. [PubMed: 11262196]

[65]. Buo AM, Stains JP, FEBS Letters 2014, 588, 1315. [PubMed: 24486014]

[66]. Paic F, Igwe JC, Nori R, Kronenberg MS, Franceschetti T, Harrington P, Kuo L, Shin D-G, Rowe DW, Harris SE, et al., Bone 2009, 45, 682. [PubMed: 19539797]

[67]. Uchihashi K, Aoki S, Matsunobu A, Toda S, Bone 2013, 52, 102. [PubMed: 22985890]

[68]. Kalajzic I, Braut A, Guo D, Jiang X, Kronenberg MS, Mina M, Harris MA, Harris SE, Rowe DW, Bone 2004, 35, 74. [PubMed: 15207743]

[69]. Galea GL, Lanyon LE, Price JS, Bone 2017, 96, 38. [PubMed: 27742499]

[70]. Zhang W, Huang Z-L, Liao S-S, Cui F-Z, Journal of the American Ceramic Society 2003, 86, 1052.

[71]. Magne D, Weiss P, Bouler J-M, Laboux O, Daculsi G, Journal of Bone and Mineral Research 2001, 16, 750. [PubMed: 11316003]

[72]. Jiao K, Niu L-N, Ma C-F, Huang X-Q, Pei D-D, Luo T, Huang Q, Chen J-H, Tay FR, Advanced Functional Materials 2016, 26, 6858.

[73]. Niu L-N, Jee SE, Jiao K, Tonggu L, Li M, Wang L, Yang Y-D, Bian J-H, Breschi L, Jang SS, et al., Nat Mater 2017, 16, 370. [PubMed: 27820813]

[74]. Kamel MA, Picconi JL, Lara-Castillo N, Johnson ML, Bone 2010, 47, 872. [PubMed: 20713195]

[75]. Cheng B, Kato Y, Zhao S, Luo J, Sprague E, Bonewald LF, Jiang JX, Endocrinology 2001, 142, 3464. [PubMed: 11459792]

[76]. Westbroek I, Ajubi NE, Alblas MJ, Semeins CM, Klein-Nulend J, Burger EH, Nijweide PJ, Biochemical and Biophysical Research Communications 2000, 268, 414. [PubMed: 10679219]

[77]. Klein-Nulend J, Van der Plas A, Semeins CM, Ajubi NE, Frangos JA, Nijweide PJ, Burger EH, The FASEB Journal 1995, 9, 441. [PubMed: 7896017]

[78]. Swartzlander MD, Blakney AK, Amer LD, Hankenson KD, Kyriakides TR, Bryant SJ, Biomaterials 2015, 41, 79. [PubMed: 25522967]

[79]. You J, Yellowley CE, Donahue HJ, Zhang Y, Chen Q, Jacobs CR, J. Biomech. Eng. 2000, 122, 387. [PubMed: 11036562]

[80]. Rath Bonivtch A, Bonewald LF, Nicolella DP, Journal of Biomechanics 2007, 40, 2199. [PubMed: 17196968]

[81]. You L, Cowin SC, Schaffler MB, Weinbaum S, Journal of biomechanics 2001, 34, 1375. [PubMed: 11672712]

[82]. Han Y, Cowin SC, Schaffler MB, Weinbaum S, Proceedings of the national academy of sciences 2004, 101, 16689.

[83]. Smalt R, Mitchell FT, Howard RL, Chambers TJ, American Journal of Physiology-Endocrinology And Metabolism 1997, 273, E751.

[84]. Kim Y-J, Bonassar LJ, Grodzinsky AJ, Journal of Biomechanics 1995, 28, 1055. [PubMed: 7559675]

[85]. Chan EP, Deeyaa B, Johnson PM, Stafford CM, Soft Matter 2012, 8, 8234.

[86]. Rakovsky A, Marbach D, Lotan N, Lanir Y, J. Appl. Polym. Sci. 2009, 112, 390.

[87]. Bush BG, Shapiro JM, DelRio FW, Cook RF, Oyen ML, Soft Matter 2015, 11, 7191. [PubMed: 26255839]

[88]. Goulet GC, Cooper DML, Coombe D, Zernicke RF, Computer Methods in Biomechanics and Biomedical Engineering 2008, 11, 379. [PubMed: 18568832]

[89]. Ishihara Y, Kamioka H, Honjo T, Ueda H, Takano-Yamamoto T, Yamashiro T, Journal of Bone and Mineral Research 2008, 23, 350. [PubMed: 17997713]

[90]. Lee CM, Genetos DC, You Z, Yellowley CE, Journal of Cellular Physiology 2007, 212, 182. [PubMed: 17370287]

[91]. Tamplen M, Fowler T, Markey J, Knott PD, Suva LJ, Alliston T, Head & Neck 2018, 40, 1453. [PubMed: 29522281]

[92]. Fowler TW, Acevedo C, Mazur CM, Hall-Glenn F, Fields AJ, Bale HA, Ritchie RO, Lotz JC, Vail TP, Alliston T, Scientific Reports 2017, 7, 44618. [PubMed: 28327602]

[93]. Sharma D, Ciani C, Marin PAR, Levy JD, Doty SB, Fritton SP, Bone 2012, 51, 488. [PubMed: 22634177]

[94]. Pathak JL, Bakker AD, Luyten FP, Verschueren P, Lems WF, Klein-Nulend J, Bravenboer N, Calcif Tissue Int 2016, 98, 596. [PubMed: 26887974]

[95]. Aziz AH, Wahlquist J, Sollner A, Ferguson V, DelRio FW, Bryant SJ, Journal of the Mechanical Behavior of Biomedical Materials 2017, 65, 454. [PubMed: 27664813]

[96]. Aziz AH, Bryant SJ, Biotechnology and Bioengineering n.d, 0, DOI 10.1002/bit.26957.

[97]. Nicodemus GD, Bryant SJ, Journal of Biomechanics 2008, 41, 1528. [PubMed: 18417139]

[98]. Nicodemus GD, Bryant SJ, Osteoarthritis and Cartilage 2010, 18, 126. [PubMed: 19748607]

[99]. Villanueva I, Hauschulz DS, Mejic D, Bryant SJ, Osteoarthritis and Cartilage 2008, 16, 909. [PubMed: 18203631]

[100]. Steinmetz NJ, Bryant SJ, Acta Biomaterialia 2011, 7, 3829. [PubMed: 21742067]

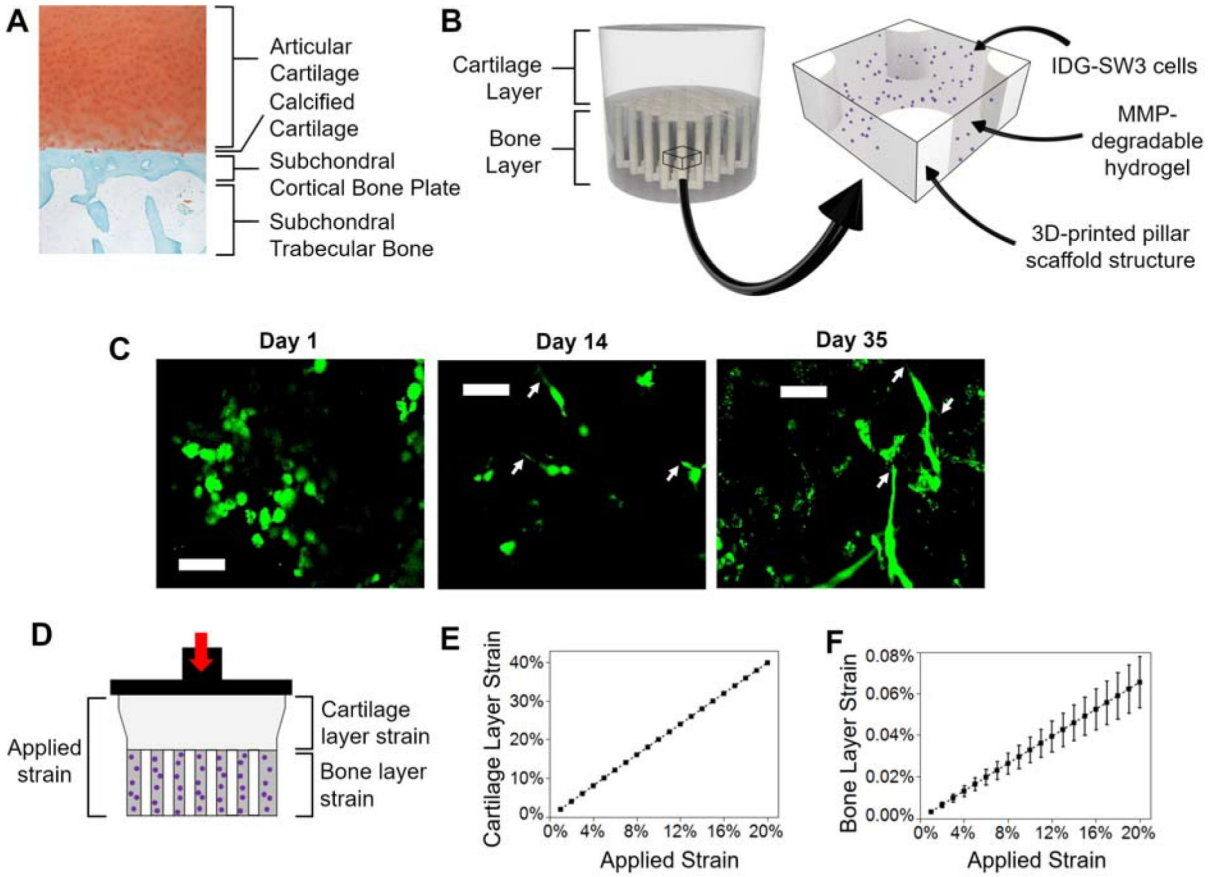

Figure 1. A bilayer composite hydrogel was designed to mimic the osteochondral unit and achieve near-physiological levels of strain in the bone layer.

(A) Representative healthy human osteochondral tissue stained with Safranin-O Fast Green. **(B)** Schematic of the bilayer composite hydrogel. The cartilage layer is comprised of a soft, acellular, non-degradable hydrogel. An enlarged section shows the different components of the bone layer: IDG-SW3 cells (purple) encapsulated in a soft, MMP-degradable hydrogel, which is a continuous matrix infill of the 3D-printed pillar scaffold structure. **(C)** Representative images of live cells stained green by Calcein-AM, scale bar is 50 μm. Arrows denote dendrite-like cellular protrusions. **(D)** Schematic of the strain in each layer with an applied strain. **(E)** Cartilage and **(F)** bone layer strain as a function of applied strain (n=4).

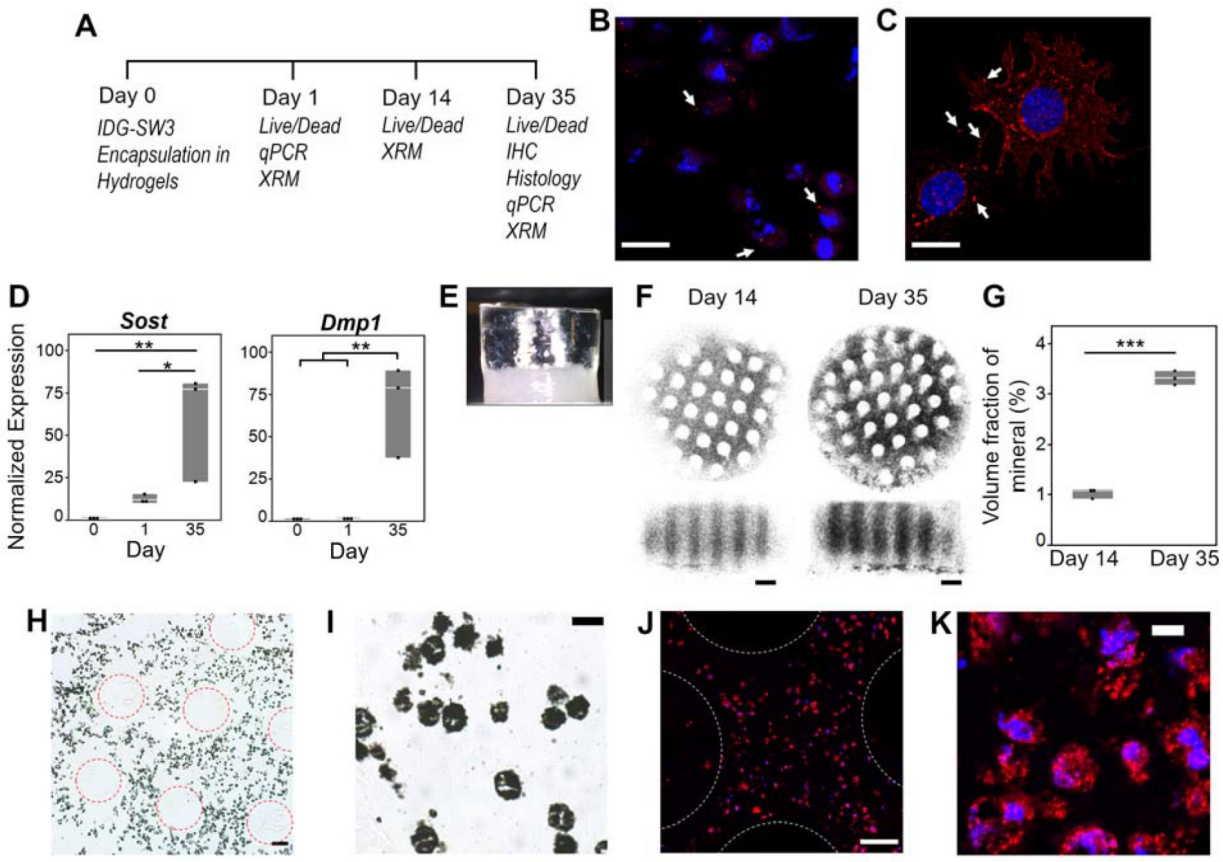

Figure 2. IDG-SW3 cells differentiated towards mature osteocytes and deposited bone matrix within the bilayer composite hydrogel.

(A) Study design and corresponding assays at each time point. **(B-C)** Representative confocal microscopy images of Connexin 43 (red, denoted with arrows) counterstained with DAPI for nuclei (blue) on (B) day 35 within hydrogel by immunohistochemistry and (C) day 3 on collagen type I coated glass dish by immunocytochemistry, scale bar = 20 μm. **(D)** Normalized gene expression (to Day 0) of osteocyte-marker genes *Dmp1* and *Sost* on Days 0 (pre-encapsulated cells), 1, and 35 (n=3). **(E)** Photograph of bilayer composite at Day 35 depicting a translucent cartilage layer and opaque bone layer. **(F)** Representative 3D X-Ray Microscope (XRM) images show mineralization (black) on days 14 and 35. At day 1, there was no detectable mineral content and hence an image was not included. **(G)** Volume fraction of mineral content from the XRM images (n=3). **(H-K)** Representative images of day 35 Glycol methacrylate-embedded sections stained with von Kossa for mineralization (black) (H-I) and for collagen type I (red) and counterstained with DAPI for nuclei (blue) (J-K). Scale bar = 100 μm (H, J), 20 μm (I), 10 μm (K). In (H) and (J) 3D-printed pillar regions are outlined with dotted circles. Symbols denote significance from post hoc Tukey's test (D) or two-sided t-test (G): * $p<0.05$; ** $p<0.01$; *** $p<0.001$.

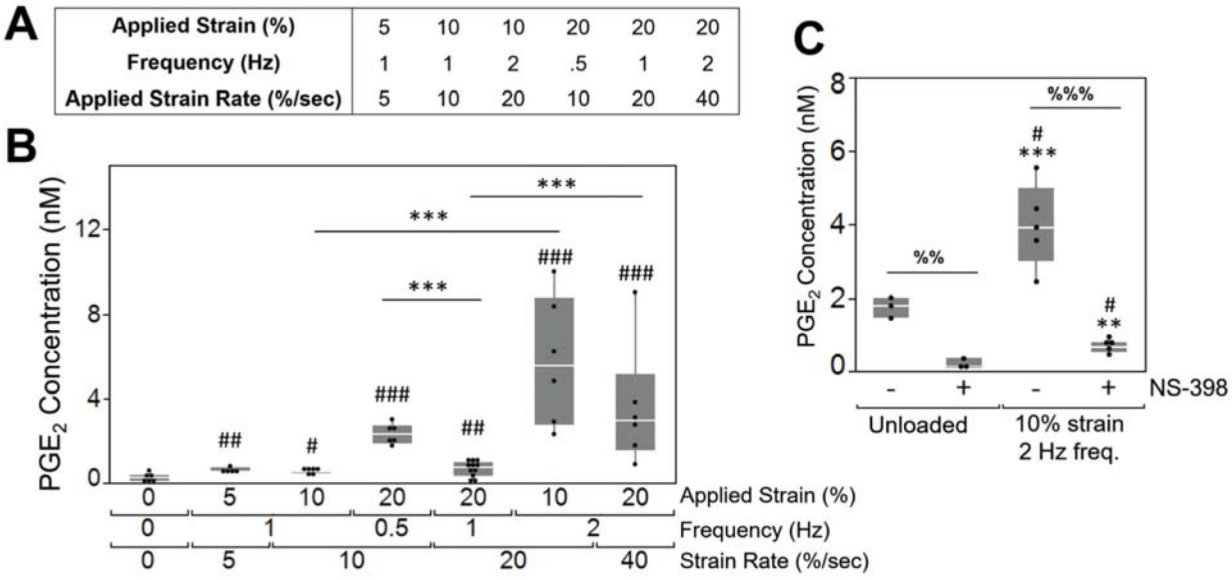

Figure 3. Osteocytes could sense and respond to loading within the bilayer composite hydrogel.

(A) Experimental loading regimes. **(B)** PGE_2 concentration in the media directly after loading as a function of applied strain, frequency, and applied strain rate. Outliers were removed and experimental sample size of all groups was 6, except for the 20% applied strain/1 Hz frequency condition which represents a sample size of 12. Symbols denote significance of post hoc Tukey's test: # compared to unloaded condition; * between strain-matched or frequency-matched conditions. **(C)** PGE_2 in the media was analyzed directly after loading (n=5) or in unloaded controls (n=3) with or without NS-398, a COX2 inhibitor. Symbols denote significance of post hoc Tukey's test: # compared to unloaded -NS-398, * compared to unloaded +NS-398; % between NS-398 treatment within the same loading condition. Significance levels: one symbol $p<0.05$; two symbols $p<0.01$; three symbols $p<0.001$.